Journal Title : Journal of Systems and Control Engineering

Article Number : 468545

Dear Author/Editor,

Greetings, and thank you for publishing with SAGE. Your article has been copyedited and typeset, and if we have any queries for you they are listed below. Please address these queries when you return your proof corrections. Thank you for your time and effort.

IMPORTANT: Please ensure that you have obtained and enclosed all necessary permissions for the reproduction of artistic works, (e.g. illustrations, photographs, charts, maps, other visual material, etc.) not owned by yourself, and ensure that the Contribution contains no unlawful statements and does not infringe any rights of others, and agree to indemnify the Publisher, SAGE Publications Ltd, against any claims in respect of the above warranties and that you agree that the Conditions of Publication form part of the Publishing Agreement.

Any colour figures have been incorporated for the on-line version only. Colour printing in the journal must be arranged with the Production Editor, please refer to the figure colour policy outlined in the email. Please assist us by clarifying the following queries:

No.	Query	Author reply
Q1	The article appears black and white in print. Please check the keynotes/legends in color in Figures 5 and 6 and change if required.	
Q2	Please check whether the edit made to the article title is correct.	
Q3	Please check whether the author names are correct as inserted.	
Q4	Please check whether the corresponding author details are correct as inserted.	
Q5	Please check whether the edits made to the sentence 'The L_1 FCS designed for this application ...' are correct.	
Q6	Please note that the variables are roman in the artworks of Figures 3 and 10, whereas italicized in text. Please check and change in artworks, if required.	
Q7	Please check whether the edits made to the sentence beginning 'These two studies also provide formal guidelines ...' are correct.	
Q8	Please note that both the terms 'criteria and constraints' and 'criteria constraints' have been used throughout the text. Please check.	
Q9	Per journal style, notes are not allowed; hence, note 7 has been incorporated within the text. Please check.	

Q10	Please note that both 'AirSTAR GTM' and 'GTM AirSTAR' have been used. Please check.	
Q11	Please confirm whether the given funding statement is accurate and correct.	
Q12	Please provide location and date of conference and publisher details for Ref. 1.	
Q13	Please provide date of conference and publisher details for Ref. 2.	
Q14	Please provide date of conference and publisher details for Ref. 3.	
Q15	Please provide location and date of conference and publisher details for Ref. 5.	
Q16	Please provide publisher details for Ref. 8.	
Q17	Please provide date of conference and publisher details for Ref. 9.	
Q18	Please provide date of conference and publisher details for Ref. 10.	
Q19	Please provide publisher details for Ref. 11.	
Q20	Please provide publisher details for Ref. 12.	
Q21	Please provide publisher location details for Ref. 13.	
Q22	Please check whether reference details are correct as given for Ref. 14.	
Q23	Please provide date of conference and publisher details for Ref. 15.	
Q24	Please provide editor(s) name, publisher location details and page range for Ref. 16.	
Q25	Please provide date of conference and publisher details for Ref. 20.	
Q26	Please provide date of report and publisher location details for Ref. 21.	
Q27	Please provide date and month of conference and publisher details for Ref. 22.	

Original Article

Institution of MECHANICAL ENGINEERS

Journal of SYSTEMS AND CONTROL ENGINEERING

Proc IMechE Part I:
J Systems and Control Engineering
0(0) 1–15

DOI: 10.1177/0959651812468545
pii.sagepub.com
SAGE

AQ1 AQ2

Multicriteria analysis of an $\mathcal{L}_1$ adaptive flight control system

AQ3 **Vladimir N Dobrokhodov[1], Enric M Xargay[2], Naira Hovakimyan[2], Isaac I Kaminer[1], Chengyu Cao[3] and Irene M Gregory[4]**

Abstract

This article presents an overview of the application of the parameter space investigation method for the multicriteria design optimization of the $\mathcal{L}_1$ adaptive flight control system implemented on the two-turbine-powered dynamically scaled generic transport model Airborne Subscale Transport Aircraft Research aircraft. In particular, this study addresses the improvement of a nominal *prototype* solution, obtained using basic design guidelines of $\mathcal{L}_1$ adaptive control theory. The results validate the theoretical claims of $\mathcal{L}_1$ adaptive control in terms of closed-loop performance and robustness and illustrate the systematic character of its design procedure. Furthermore, this article shows the suitability of the parameter space investigation method for the multicriteria design optimization over a multidimensional design variable space of a flight control system subject to desired control specifications. The use of this particular method is of special interest, as it provides invaluable information about the behavior of the closed-loop system in an extended space of design parameters and performance criteria. The results and conclusions of this article have led to a deeper understanding of the characteristics of the closed-loop adaptive system and have contributed to the improvement of the flying qualities and the robustness margins of the adaptive $\mathcal{L}_1$-augmented aircraft, which has been recently flight tested by National Aeronautics and Space Administration.

Keywords

$\mathcal{L}_1$ adaptive control, flying qualities, multicriteria optimization, Pareto optimality, quasi-random sequences

Date received: 26 February 2012; accepted: 29 October 2012

Introduction

Adaptive control has long been seen as an appealing technology to improve aircraft performance with reduced pilot compensation in adverse flight conditions or in the event of control surface failures and vehicle damage. Under these conditions, which are characterized by a high degree of uncertainty with respect to a nominal aircraft, the achievable levels of performance and flying qualities (FQ) that a nonadaptive flight control system (FCS) can provide might be limited. However, several limitations of the conventional adaptive systems have prevented this technology from being widely used in safety-critical aerospace applications.[1–3] In particular, the key deficiencies of conventional adaptive (flight) control systems can be summarized as follows: (1) the lack of transient characterization of the closed-loop response, (2) the limited framework for analysis of the robustness and performance properties of closed-loop adaptive systems, and (3) the lack of systematic design guidelines to solve the trade-off between adaptation, performance, and robustness.

The theory of $\mathcal{L}_1$ adaptive control overcomes the limitations of conventional adaptive control architectures described above and enables the design of robust adaptive control architectures using fast adaptation schemes.[4] The key feature of $\mathcal{L}_1$ adaptive control is the decoupling of the adaptation loop from the control loop, which enables fast adaptation without sacrificing robustness. In fact, in $\mathcal{L}_1$ adaptive control architectures, the rate of the adaptation loop can be set arbitrarily

[1]Department of Mechanical and Aerospace Engineering, Naval Postgraduate School, Monterey, CA, USA
[2]Department of Aerospace Engineering, University of Illinois at Urbana-Champaign, Urbana, IL, USA
[3]Department of Mechanical Engineering, University of Connecticut, Storrs, CT, USA
[4]Dynamics Systems and Control Branch, NASA Langley Research Center, Hampton, VA, USA

Corresponding author:
Vladimir N Dobrokhodov, Department of Mechanical and Aerospace Engineering, Naval Postgraduate School, Monterey, CA 93943, USA. AQ4
Email: vldobr@nps.edu

high, subject only to hardware limitations (computational power and high-frequency sensor noise), while the trade-off between performance and robustness can be addressed via conventional methods from classical and robust control. Fast adaptation enables compensation for the undesirable effects of rapidly varying uncertainties and significant changes in system dynamics and is thus critical toward achieving guaranteed transient performance without enforcing persistency of excitation or resorting to high-gain feedback. Moreover, the $\mathcal{L}_1$ adaptive control theory provides design guidelines that significantly reduce the tuning effort of the adaptive controller.

The main challenge for the design of $\mathcal{L}_1$ FCSs is the optimal tuning of its elements to provide desired FQ with satisfactory robustness margins over large operational envelopes and uncertainty scenarios. While the theory of $\mathcal{L}_1$ adaptive control provides basic design guidelines to address the trade-off between performance and robustness, optimization of the design of $\mathcal{L}_1$ adaptive controllers is still largely open and hard to address. The main difficulty is the nonconvex and nonsmooth nature of the underlying optimization problem that involves the $\mathcal{L}_1$-norm of cascaded linear systems. Randomized parametric algorithms have been proven to be effective in control-related nonconvex optimization problems, and therefore they seem attractive for the optimal design of $\mathcal{L}_1$ adaptive controllers.[4,5] In particular, one of the approaches that can help to solve this multiobjective optimization problem is the parameter space investigation (PSI) method.[6,7] This method explicitly addresses the issues associated with high dimensionality of the criteria and the functional constraint spaces. It takes into account the complexity and the computational expenses of sampling the design space of high dimensionality by employing the quasi-random sampling (LP-tau sequences, see Statnikov and Matusov,[6] Sobol and Statnikov,[7] and references therein), which yield converging results by a factor of 4–8 smaller sample sizes compared to the other methods. The method is implemented in a user-friendly and "model agnostic" software package called Multicriteria Optimization and Vector Identification (MOVI).[8]

In this article, we take advantage of the design guidelines of $\mathcal{L}_1$ adaptive control for the design optimization of the $\mathcal{L}_1$ FCS implemented on the generic transport model (GTM), which is part of the Airborne Subscale Transport Aircraft Research (AirSTAR) system at the National Aeronautics and Space Administration (NASA) Langley Research Center.[9,10] In particular, this study addresses the application of the PSI method for the construction of the feasible solution set and for the subsequent improvement of a nominal prototype design. This article demonstrates that the consistent application of the design guidelines of $\mathcal{L}_1$ adaptive control becomes particularly beneficial for the construction of the feasible solution set. In fact, the ability to systematically adjust the control parameters in $\mathcal{L}_1$ adaptive architectures considerably simplifies the identification of a nominal feasible solution from which to start the search for other feasible solutions and the subsequent extension of the feasible solution set. The availability of an initial feasible solution may narrow the design variable (DV) space over which the search for feasible solutions should be performed. Furthermore, considering the benefits of sampling the multidimensional DV space by the LP-tau quasi-random sequences, the number of trials required for the construction of the feasible set may be significantly reduced.

This article illustrates the suitability of the PSI method as a tool for formulating and solving multicriteria optimization problems for design of adaptive FCS. The work reported here is not intended to compare the benefits and drawbacks of various optimization methods; instead, it illustrates the complexity of multicriteria analysis and suggests a viable approach to the design of control systems for safety-critical applications. An explicit comparison of various multicriteria analysis methods can be found in the study by Sobol and Statnikov,[7] which provides an essential overview of modern approaches to multicriteria decision making.

This article is organized as follows. Section "NASA AirSTAR and $\mathcal{L}_1$ flight control law" introduces the design framework consisting of the GTM aircraft model, the adaptive control law, and the optimization method. This section starts with an overview of the NASA AirSTAR facility and the $\mathcal{L}_1$ flight control law developed for the GTM aircraft; in addition, it presents the nominal prototype design, with its main performance and robustness properties. This section also formulates the multiobjective optimization task and provides a brief discussion that justifies the choice of the optimization method. Section "Formulation of the optimization problem" formulates the FCS design optimization problem and provides a brief discussion of the PSI numerical implementation and the workflow of the optimization process. The design optimization of the $\mathcal{L}_1$ FCS for the GTM aircraft is addressed in section "Solutions and analysis." In particular, this section provides a detailed discussion of the different steps of the optimization process, including the construction of the feasible solution and the improvement of the prototype design. Finally, section "Conclusion" summarizes the key results and contains the main conclusions.

NASA AirSTAR and $\mathcal{L}_1$ flight control law

AirSTAR facility

During 2007–2010, the NASA's Aviation Safety Program created the Integrated Resilient Aircraft Control (IRAC) project with the objective of advancing and transitioning adaptive flight control technologies to increase aviation safety. The IRAC project had special interest in piloted flight under adverse flight conditions such as unusual attitudes, control surface failures, icing, and structural damage. As part of the project,

Figure 1. GTM AirSTAR unmanned aircraft and its full-scale prototype.

NASA developed AirSTAR, a state-of-the-art facility designed for the purpose of investigating and validating high-payoff technologies aimed at the loss-of-control problem using remotely piloted subscale models without excessive risk.[9,10] The primary flight test vehicle of AirSTAR is the GTM tail number T2, which is shown in Figure 1. The T2 is a twin-engine jet-powered and dynamically scaled (5.5%) civil transport aircraft that was designed and instrumented to perform control law evaluation, experiment design, and modeling research, in-flight failure emulation and flight in upset conditions.

The AirSTAR facility also incorporates a high-fidelity nonlinear simulation of the GTM aircraft. The GTM vehicle has been extensively tested in the NASA Langley wind tunnels with particular emphasis on modeling nonlinear regions of the extended flight envelope well beyond nominal flight as well as developing a database for a number of structural damage scenarios.[11,12] With this capability, AirSTAR provides a common research environment for both simulation and flight. In this article, we take advantage of the high-fidelity nonlinear model of the GTM vehicle for the design of the $\mathcal{L}_1$ flight control law.

$\mathcal{L}_1$ flight control law for the GTM aircraft

The $\mathcal{L}_1$ flight control law developed for the AirSTAR flight test vehicle has as its primary objective achieving reliable tracking for a variety of tasks with guaranteed stability and robustness in the presence of uncertain dynamics, such as changes due to rapidly varying flight conditions during standard maneuvers, and unexpected failures. All these requirements are expected to be reached while providing Level 1 FQ[13,14] under nominal flight conditions, with a graceful degradation under significant adversity.

The $\mathcal{L}_1$ FCS designed for this application consists of a nonadaptive stability augmentation system (SAS) for pitch and roll and adaptive control augmentation system (CAS) for a three-axes angle of attack (AOA, α), roll rate (p), and angle of sideslip (AOSS, β). The $\mathcal{L}_1$ adaptive controller provides thus command-tracking capabilities in both nominal and off-nominal conditions as there is no nonadaptive CAS baseline to assist it. The $\mathcal{L}_1$ CAS consists of two decoupled $\mathcal{L}_1$ controllers, one for the longitudinal channel and another one for control of the lateral–directional dynamics. The implemented longitudinal $\mathcal{L}_1$ controller utilizes feedback in AOA and pitch rate to generate an elevator control signal in order to track AOA reference signal. The lateral/directional $\mathcal{L}_1$ controller uses feedback in AOSS, roll rate, and yaw rate to generate aileron and rudder commands in order to track sideslip-angle and roll-rate reference signals with reduced coupling. In the current $\mathcal{L}_1$ FCS, the pilot adjusts directly the thrust level using the throttle lever. An interested reader is referred to the study by Xargay et al.[15,16] for a more detailed explanation of the $\mathcal{L}_1$ FCS implemented on the NASA AirSTAR flight test vehicle.

The design of the longitudinal $\mathcal{L}_1$ FCS is based on the linearized short-period dynamics of the GTM at the reference flight condition (80 kt, 1000 ft). Since the airplane is Level 1 FQ at this flight condition, the desired dynamics of the *state predictor* are chosen to be close to those of the actual aircraft. For the nominal prototype design, the natural frequency of the poles of the system is reduced from 6 to 5.5 rad/s, while the damping ratio is increased from 0.47 to 0.85. A first-order low-pass filter with direct current (DC) gain 1 and a bandwidth of 20 rad/s was used in the matched contribution to the elevator command, while two cascaded first-order low-pass filters were used in the unmatched channel, both having DC gain equal to 1 and bandwidths of 5 and 7 rad/s, respectively. Finally, the adaptation sampling time was set to 600 Hz, which corresponds to the fastest integration cycle allowed in the AirSTAR flight control computer. A first-order prefilter with bandwidth of 20 rad/s was added to shape the pilot command. The $\mathcal{L}_1$ FCS, with its main elements as well as the DVs, is represented in Figure 2. This *prototype* design of the state predictor, the low-pass filters, the adaptation sampling rate, and the prefilter, delivers an AOA response similar to the desired one (α_{des}) (Figure 3). The deviation of the AOA response from the commanded step is due to the phugoid mode of the aircraft, which is stable, oscillatory, and slow. This phugoid deviation appears when designing AOA and pitch-rate CASs and can be easily compensated for by the pilot (or autopilot in the case of autonomous flight). The nominal design ensures a time-delay margin of the inner loop of approximately 85 ms and a gain margin of 7.2 dB, in wings-level flight at the reference flight condition. At this flight condition, the FQ are predicted to be Level 1, and the FCS design has no predicted pilot-induced oscillation (PIO) tendencies (for an acquisition time of 1.5 s). Naturally, these metrics correspond to specific performance criteria, and these initial nominal values will be used as reference values for the definition of the criteria constraints during the optimization process.

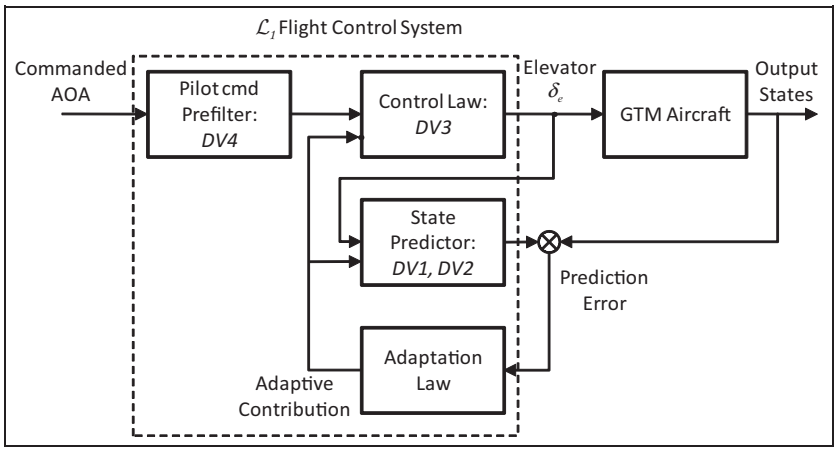

Figure 2. Longitudinal channel of the $\mathcal{L}_1$ flight control architecture.
AOA: angle-of-attack; GTM: generic transport model.

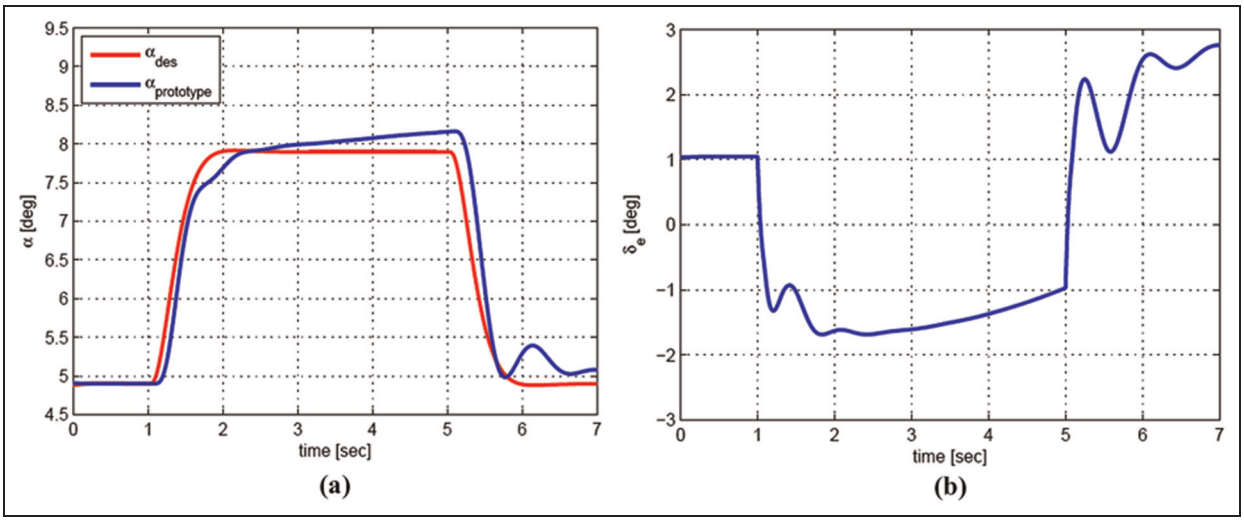

Figure 3. Prototype design. 3° AOA step response. (a) Angle of attack, α and (b) elevator deflection, δ_e.

AQ6

Multicriteria optimization framework

The objective of the adaptive controller tuning task is to find an optimal solution in the multidimensional controller parameter space that minimizes the difference between the desired and actual responses of the airplane, while ensuring satisfactory FQ, desired robustness margins, and reasonable actuator activity. It is clear that the task belongs to the class of multicriteria optimization problem. A general multiobjective design problem can be posed as follows. Minimize a vector $\mathbf{F}(\mathbf{x})$ of k objective functions $F_k(\mathbf{x})$

$$\min_{\mathbf{x}} \mathbf{F}(\mathbf{x}) = [F_1(\mathbf{x}), F_2(\mathbf{x}), \ldots, F_k(\mathbf{x})]^T$$

subject to $g_i(\mathbf{x}) \leqslant 0, \quad i = 1, 2, \ldots, m$ and $h_j(\mathbf{x}) = 0$, $j = 1, 2, \ldots, e$, where m is the number of inequality constraints, e is the number of equality constraints, and $\mathbf{x} \in E^n$ is a vector of DVs. The feasible solution set $\mathbf{X}$ is defined as $\{\mathbf{x} | g_i(\mathbf{x}) \leqslant 0, i = 1, 2, \ldots, m$ and $h_j(\mathbf{x}) = 0$, $j = 1, 2, \ldots, e\}$, and the feasible criterion space $\mathbf{Z}$ (also called attainable set) is defined as the set $\{\mathbf{F}(\mathbf{x}) | \mathbf{x} \in \mathbf{X}\}$. Feasibility of a design vector $\mathbf{x}$ implies that no constraint is violated. Attainability of a criteria vector implies that a point in the criterion space maps to a unique point in the design space. Optimality of solutions is defined in terms of Pareto dominance; the Pareto set consists of solutions that are not dominated by any other solutions. For more details on the fundamental definitions and properties of the Pareto optimality, the interested reader is referred to the monograph.[7]

The task of the $\mathcal{L}_1$ adaptive controller optimization consists of a mixture of numerical simulation (GTM aircraft) and analytical calculations (adaptive controller design and its performance metrics) where there is no easy way of calculating derivatives of the objective functions. Therefore, nongradient optimization methods are better candidates for this problem; another

important advantage of these methods is that they are more likely to find global optima and not to be stuck on local ones, in contrast to gradient methods. The classification of nongradient methods[17] designed to tackle this kind of problem is usually based on the stage when the decision-making process applies the preferences on the objectives: never, before, during, or after the actual optimization process. In contrast to many of the existing approaches, the PSI method enables a very powerful interactive articulation of preferences via a "dialog" with the designer. The key advantages of this approach are as follows: (1) there is no need for a priori preference information, (2) only local preference information is needed, and (3) it is a learning process where the decision making improves the understanding of the problem, thus making these trade-offs visible. Disadvantages include the following: (1) the solutions depend on how well the preferences are articulated and (2) the required computational effort is high and depends on the complexity of the underlying problem.

Another significant advantage of the PSI method is that it accounts for a possibility of computational instability of the Pareto-optimal set when even small errors in the criteria $\mathbf{F}(\mathbf{x})$ may lead to drastic change of the feasible solution set $\mathbf{X}$. For problems that are neither linear nor concave, the key methods for the Pareto optimality utilize two major approaches: (1) minimization of various functions representing specific metrics (e.g. Hausdorff, see Sobol and Statnikov[7]) and (2) covering the feasible solution set with subsets of a specific shape (cubes, spheres, etc.). The PSI method falls within the second category, employing uniformly distributed pseudorandom sequences of points that guarantee the fastest convergence to the Pareto-optimal approximation. In particular, the LP-tau sequences are used as a sampling mechanism to cover the DV space. It is also important that the PSI method does not alter the optimization task by "mapping" a set of multiple criteria to just one scalar functional. Details of the PSI realization can be found in the study by Sobol and Statnikov,[7] while comprehensive overviews of multiobjective optimization approaches are discussed in the studies by Andersson[17] and Marler and Arora.[18] These two studies also provide formal guidelines on the choice of the most suitable method for particular optimization problems.

To support this multicriteria approach, the MOVI package provides a rich set of analysis tools. Besides numerical results organized as a test table, it provides a number of visual tools. In particular, histograms of DVs, criterion versus DV plots, and criterion versus criterion plots are the most intuitive and effective tools used during the interactive analysis. A comprehensive introduction to the effective use of the MOVI package can be found in the studies by Statnikov and Matusov[6] and Sobol and Statnikov.[7]

The PSI-based optimization methodology proposed in this work contains two steps. First, taking the prototype solution as a reference design, the PSI method is used for the construction of the *feasible solution set* and for determining a direction of improvement for the design of the FCS. This first step is based on a reduced and relaxed set of criteria and constraints. Then, at the second stage, the PSI method is again used to determine an *optimal design* that satisfies an extended set of performance and robustness constraints and improves the initial reference prototype.

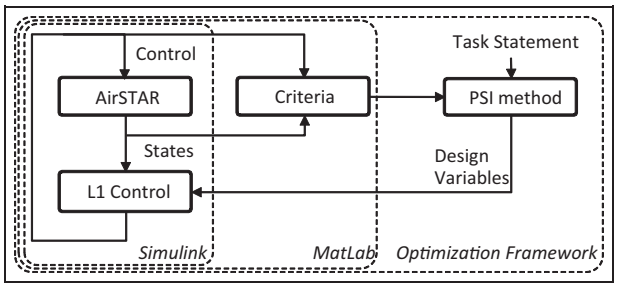

Figure 4. Optimization framework.
AirSTAR: Airborne Subscale Transport Aircraft Research; PSI: parameter space investigation.

The architecture of the developed optimization framework is presented in Figure 4. The framework integrates the GTM model and the $\mathcal{L}_1$ adaptive controller (both implemented in Simulink), the criteria calculating scripts (implemented in MATLAB), and the PSI method (implemented by the MOVI software). This setup allows integrating the capabilities of a high-fidelity simulation environment with the vast set of features of the MOVI package.

We note that although both the PSI and the software package MOVI have been developed to address problems with high dimensionality of both the design and the criteria spaces, for the sake of clarity, we keep the design problem within a reasonable complexity. Thus, the design procedure is only applied to the design of the longitudinal channel. Finally, we also note that all the results included in this study are obtained by the MOVI software package combined with the MATLAB environment[19] and are based on the full nonlinear simulation model of the two-engine-powered dynamically scaled GTM AirSTAR system, which was released by NASA in December 2009.

Formulation of the optimization problem

This section presents the formulation of the $\mathcal{L}_1$ FCS design optimization problem, indicating the sets of DVs and criteria considered in this study, as well as the criteria constraints to be satisfied.

DVs and criteria

DVs. Since the primary objective is to improve the FQ of the prototype design while guaranteeing satisfactory robustness margins, we include the natural frequency

and the damping ratio of the eigenvalues of the state-predictor dynamics (which can speed up or slow down the response of the augmented aircraft) and the bandwidth of the low-pass filter in the matched channel (which can be used to adjust the time-delay margin of the control loop) as DVs (Figure 2). Furthermore, we also consider the optimization of the bandwidth of the pilot-command prefilter, which can be used to shape the pilot command as to prevent elevator rate limiting and avoid structural mode–flight interaction. The following list summarizes the set of optimization parameters that define the DV space.

- *DV1*. Natural frequency of the state-predictor eigenvalues (rad/s).
- *DV2*. Damping ratio of the state-predictor eigenvalues (dimensionless).
- *DV3*. Bandwidth of the "matched" low-pass filter (rad/s).
- *DV4*. Bandwidth of the pilot-command prefilter (rad/s).

Criteria and pseudocriteria. The set of design criteria considered in this study is chosen to evaluate performance and robustness properties of the GTM aircraft augmented with the $\mathcal{L}_1$ FCS. To provide an adequate assessment of the performance characteristics and FQ of the $\mathcal{L}_1$-augmented aircraft, both pilot-off-the-loop and pilot-in-the-loop performance metrics are included in the design procedure. The metrics considered can thus be classified into the following three categories.

1. Pilot-off-the-loop performance metrics.
2. Robustness metrics.
3. FQ and PIO metrics.

Because the present material addresses only the design of the longitudinal channel of the $\mathcal{L}_1$ FCS, the set of metrics used in this study is mainly based on the (time-domain) longitudinal response of the GTM with the $\mathcal{L}_1$ FCS closing the loop. We note that some of the metrics used in this study were also proposed in the study by Stepanyan et al.[20] for the evaluation of aircraft augmented with adaptive FCSs.

Pilot-off-the-loop performance metrics. This first set of metrics evaluates the performance of the augmented aircraft by characterizing its response to step inputs. In particular, the pilot-off-the-loop performance metrics are based on the time-domain response to an AOA step command of 3° held for 4 s (Figure 3), starting from a wings-level flight condition. The metrics capture the deviation of the actual response of the aircraft from a given desired response, which is defined to provide satisfactory FQ without reaching the physical limits of the platform, as well as different measures of control activity, load factor, and cross-coupling. We note that in this study, all metrics are normalized to the amplitude of the step command considered (3°).

Next, we provide a description of the metrics included in this study. First, however, we need to introduce key notations to facilitate the definition of these metrics. Along with the previously defined AOA (α) and AOA desired response (α_{des}), α_{cmd} is used here to denote the AOA pilot command; β_{des} is the AOSS desired response; p_{des} is the roll-rate desired response; A_z is the vertical acceleration; while δ_e is the elevator deflection command. We let t_0 be the time instant at which the step command is applied and define t_f as the final time instant considered for the performance evaluation ($t_f = t_0 + 4\,\text{s}$). With the above notations, the metrics are formally defined as follows.

P1: Final deviation. This metric captures the final deviation of the actual AOA response from the desired AOA response at 4 s after the application of the step command. This metric is set to zero if the actual response reaches the AOA reference command before the end of the 4-s step

$$P1 = \begin{cases} \left|\alpha(t_f) - \alpha_{des}(t_f)\right| & \text{if } \alpha(t) < \alpha_{cmd}, \forall t \in [t_0, t_f] \\ 0 & \text{otherwise} \end{cases}$$

This metric penalizes or excludes sluggish responses.

P2: Maximum deviation from desired AOA response. This metric captures the maximum deviation (in absolute value) of the actual AOA response from the desired AOA response

$$P2 = \max_{t\in[t_0,\,t_f]} |\alpha(t) - \alpha_{des}(t)|$$

P3: Integral deviation from desired AOA response. This metric is defined as the (truncated) $\mathcal{L}_1$-norm of the deviation of the actual AOA response from the desired AOA response

$$P3 = \int_{t_0}^{t_f} |\alpha(t) - \alpha_{des}(t)|dt$$

P4: Overshoot in AOA response. This metric captures possible overshoots and low-damping characteristics in the AOA response

$$P4 = \begin{cases} \max_{t\in[t_0,\,t_f]} |\alpha(t)| & \text{if } \alpha(t) > \alpha_{cmd}, \text{for some } t \in [t_0, t_f] \\ \alpha_{cmd} & \text{otherwise} \end{cases}$$

P5: Maximum deviation from desired AOA rate response. This metric captures the maximum rate deviation (in absolute value) of the actual AOA response from the desired AOA response

$$P5 = \max_{t\in[t_0,\,t_f]} |\dot{\alpha}(t) - \dot{\alpha}_{des}(t)|$$

P6: Integral deviation from desired AOA rate response. This metric is defined as the (truncated) $\mathcal{L}_1$-norm of the rate deviation of the actual AOA response from the desired AOA response

$$P6 = \int_{t_0}^{t_f} |\dot{\alpha}(t) - \dot{\alpha}_{des}(t)|dt$$

The metrics *P1–P6* provide a good characterization of the transient response of the augmented aircraft when compared to a given desired response. Next, we present a set of metrics that can be extracted from the same step response and complement the AOA metrics defined above.

P7: Maximum vertical acceleration. Load factor (and passenger comfort) requirements can be captured by the maximum vertical acceleration during the step response

$$P7 = \max_{t\in[t_0,\,t_f]} |A_z(t)|$$

P8: Control effort. This metric is defined as the (truncated) $\mathcal{L}_1$-norm of the elevator deflection command

$$P8 = \int_{t_0}^{t_f} |\delta_e(t)|dt$$

This metric penalizes flight control designs that require a high control activity to achieve the desired control objective. It is important to note, however, that a high control effort might just be the result of a faster AOA response, and therefore a large *P8* might not always be an undesirable response characteristic.

P9: Maximum elevator rate. Excessive control rate can be identified by the following metric:

$$P9 = \max_{t\in[t_0,\,t_f]} |\dot{\delta}_e(t)|$$

This metric penalizes designs with high elevator rates in order to prevent undesirable effects from rate limiting.

P10: Maximum elevator acceleration. High-order derivatives of the control commands are coupled to the flexible modes of the aircraft. The following metric, based on the second derivative of the elevator command, captures excessive accelerations and oscillations in the control command that could potentially lead to unwanted structural mode interactions

$$P10 = \max_{t\in[t_0,\,t_f]} |\ddot{\delta}_e(t)|$$

P11: Maximum of $\mathcal{L}_1$ prediction error. This metric captures the maximum error between the actual system state and the state of the $\mathcal{L}_1$ state predictor, usually denoted by $\tilde{x}(t)$

$$P11 = \max_{t\in[t_0,\,t_f]} \|\tilde{x}(t)\|_\infty$$

In $\mathcal{L}_1$ adaptive control architectures, the accurate estimation of system uncertainties and the performance guarantees rely on the (small) "size" of the prediction error $\tilde{x}(t)$. This metric is used to monitor the correct functioning of the $\mathcal{L}_1$ adaptive controller.

P12: Maximum deviation in cross-coupling dynamics. This metric captures the lateral–directional coupling induced by a command in the longitudinal channel

$$P12 = \max_{t\in[t_0,\,t_f]} \left[|\delta_e(t)|((\beta(t) - \beta_{des}(t))^2 + (p(t) - p_{des}(t))^2)\right]$$

This metric primarily provides valuable information for the design of the lateral–directional FCS.

P13: Integral deviation in cross-coupling dynamics. This metric is the integral version of the previous cross-coupling metric and is defined as follows

$$P13 = \int_{t_0}^{t_f} |\delta_e(t)|((\beta(t) - \beta_{des}(t))^2 + (p(t) - p_{des}(t))^2)dt$$

Similar to *P12*, this metric would be more adequate for the design of the lateral–directional control system, and both metrics are included in this study only to illustrate a set of additional metrics that can be derived from the response of the augmented aircraft to a command in the longitudinal channel.

Robustness margins. In this preliminary study, the only robustness metric considered for optimization is the *time-delay margin* of the closed-loop adaptive system. It is defined at the input of the aircraft (time delay inserted at the elevator deflection command), and it is derived from the time-domain response of the augmented aircraft. For a given wings-level flight condition and with the pilot-off-the-loop, a small perturbation in the trim (initial) condition is introduced. The time-delay margin is determined as the minimum time delay that produces sustained oscillations in the AOA response as the $\mathcal{L}_1$ FCS tries to stabilize the aircraft at the given trim condition. In this study, this robustness metric will be denoted by *R1*. Note that the time delay introduced in the elevator control channel is in addition to the 25 ms that is already modeled in the AirSTAR simulation environment.

Criteria addressing FQ and PIO characteristics. Finally, predictions for both FQ and PIO tendencies have also been included in order to complement the pilot-off-the-loop performance metrics presented above. For this study, we consider the time-domain Neal–Smith (TDNS) FQ and PIO criteria, which were specifically developed for nonlinear aircraft dynamics and nonlinear FCS. For a detailed description of this criterion, an interested reader is referred to the study by Bailey and Bidlack.[21] The reader can also find in Choe et al.[22]

a study on the prediction of FQ and adverse pilot interactions in the GTM augmented with the $\mathcal{L}_1$ FCS. We use four different metrics, extracting all of them from the TDNS criterion for an acquisition time of 1.5 s, to characterize the FQ and PIO tendencies of the augmented aircraft:

FQ1: Tracking performance. In the TDNS criterion, the root-mean-squared tracking error is used to evaluate the closed-loop performance with the pilot-in-the-loop. A value of zero means that the pilot is able to perfectly track (with zero error) the reference command after the specified acquisition time.
FQ2: Pilot workload. In the TDNS criterion, the pilot workload is given by the pilot compensation phase angle (in degrees), which is derived from the optimal pilot model obtained from the criterion. A value of zero means that there is no need for either pilot lead or lag compensation.
FQ3: FQ level. The two metrics above, *FQ1* and *FQ2*, are used to determine the predicted FQ level based on the FQ boundaries proposed in the criterion. *FQ3* is a discrete metric, and it only admits the values 1, 2, and 3, which correspond to Level 1, Level 2, and Level 3 FQ, respectively.
FQ4: PIO tendency. The TDNS criterion also provides a prediction for the susceptibility of the augmented aircraft to PIO. This PIO-susceptibility metric is used to complement the FQ metrics discussed above. According to the TDNS criterion, a value above 100 implies that the augmented aircraft is PIO-prone ~~configuration~~, whereas a value below 100 indicates a PIO-immune configuration.

This set of FQ metrics will be used in section "Solutions and analysis" to improve a prototype design of the longitudinal channel of the $\mathcal{L}_1$ FCS. For the first stage of the design that aims to explore the feasibility set, only a subset of these metrics will be used. The complete set of metrics will be used in the second stage to optimize the design of the adaptive control system. Based on the objectives of the task and previous flight control design expertise, the following vectors of criteria {*P1, P2, P3, P4, P5, P6, FQ1, FQ2, FQ3, FQ4, R1*} and pseudocriteria {*P7, P8, P9, P10, P11, P12, P13*} are defined.

Criteria constraints

Based on the metrics defined, the final design of the $\mathcal{L}_1$ FCS should *ideally* verify the set of control objectives at the reference flight condition of 80 kt of (equivalent) airspeed and 1000 ft of altitude. Corresponding to these flight conditions, a set of three criteria constraints was defined a priori

$$P1 \leqslant 0.1,\ FQ3 = 1, \text{ and } P4 \leqslant 1.2.$$

The first and second conditions address directly the control specifications, namely, the final value of the step response within 10% of the desired, and the predicted Level 1 FQ. The third inequality imposes a 20% constraint on the overshoot in the step response, establishing thus a (loose) bound on the acceptable transient performance characteristics of the actual AOA response. Due to significant difficulty of defining all criteria constraints consistent with feasibility of the solution, the rest of the constraints will be identified interactively while analyzing the test tables.

Solutions and analysis

This section presents the two steps of iterative application of the PSI method to the design improvement of the longitudinal channel of the $\mathcal{L}_1$ FCS. As mentioned earlier, the first iteration uses a reduced set of the control metrics. Numerical implementation of this first step is relatively efficient with the "computational price" of one solution measured in minutes. At the second step, when using the extended set of criteria, the efficiency of numerical implementation becomes critical because the "computational price" of one solution is measured in tenths of minutes. The architecture of the optimization framework was presented in Figure 4.

First iteration: construction of the feasible solution set

The construction of the feasible solution set starts by defining test intervals for the DVs. These test intervals have been identified with respect to the nominal prototype solution obtained from the $\mathcal{L}_1$ design procedure (Table 1).

The objective of the first step is to find a direction of improvement for the nominal design. More precisely, we aim here at determining tight intervals for the DVs characterizing the state predictor (*DV1* and *DV2*) that would provide Level 1 FQ and would not deviate from the desired response defined previously. To this end, the design is to be minimized with respect to the following reduced number of criteria {*P1, P2, P3, P4, P5, P6, FQ1, FQ2*}.

The robustness metric *R1* and the PIO metric *FQ4* are not included in this first step because their

Table 1. Initial intervals of design variables.

Design variable	$\mathcal{L}_1$ prototype	Initial intervals of variation of design variables	
		Min	Max
DV1	5.50E+00	4.00E+00	8.00E+00
DV2	8.50E−01	5.00E−01	1.10E+00
DV3	2.00E+01	5.00E+00	3.00E+01
DV4	2.00E+01	1.00E+01	5.00E+01

evaluation is computationally expensive; these metrics will be considered in the next step of the optimization process when the domain of the DVs becomes significantly refined. The metrics *P7–P10* are not included in the set of criteria because improved FQ may require "high" values of these metrics. Nevertheless, they are included in the optimization process as pseudocriteria (pseudocriterion differs from a criterion by the fact that it is not included in the calculation of the Pareto front; for more details, see Statnikov and Matusov[6]) thus providing useful insights into the dynamics of the augmented aircraft. Similarly, the metric *P11*, which can be used to monitor the correct operation of the $\mathcal{L}_1$ adaptive controller, does not need to be minimized as long as it remains a couple of orders of magnitude below the system state (truncated) $\mathcal{L}_\infty$-norm. Finally, the metrics *P12* and *P13* are included for the sake of completeness and should be considered only for the design of the lateral–directional control system.

The MOVI package performs a predefined set of numerical trials and then forms a test table. Interactive work with the test table consists of sequential tightening of the DV constraints and is well supported by a number of graphical instruments implemented in MOVI. The final result achieved in this first iteration of the optimization process is based on 1024 tests. Out of these 1024 tests, 427 vectors did not satisfy the a priori given criteria constraints. The solutions that did not satisfy the constraints entered the *table of criteria failures*; every entry of this table is available for a detailed analysis. The remaining 597 vectors that did satisfy a priori given criteria constraints were used to construct the test table. While tightening the criteria constraints in the test table, the following new criteria constraints were formulated (Table 2). Note that while analyzing the test table, the constraint of *P4* was significantly tightened to the value of 1.02. Furthermore, the response on criteria *P1* is not presented in Table 2 because all solutions provided identical response, $P1 = 0$. Only 20 solutions were found to be feasible according to these criteria constraints, all of them contributing to the Pareto-optimal solutions. A fragment of the criteria table is given in Table 3.

Analysis of the criteria table shows that solution #993 is the most preferable one. This solution is equivalent to others with respect to criterion *P4*, it is superior to others over a set of five criteria {*P2, P3, P6, FQ1, FQ2*} and is weaker than the prototype only with respect to the criterion *P5*. Furthermore, the other 19 solutions are better than the prototype with respect to four criteria {*P2, P3, FQ1, FQ2*}. However, none of the solutions are superior to the prototype with respect to criterion *P5*. In particular, this observation implies that if the prototype design vector had been sampled by the system, then it would belong to the Pareto set. On the other hand, this result confirms that the solution obtained following the basic $\mathcal{L}_1$ design guidelines is near optimal for this set of criteria.

This analysis allows defining the direction of further search. In particular, the results provide tight intervals for the DVs *DV1* and *DV2* characterizing the state-predictor dynamics and suggest extending the initial intervals of variation of the DVs *DV3* and *DV4* (Figure 5). Based on these results and their analysis, a new experiment is performed with the objective to improve the feasible solution set and to determine an optimal solution of the $\mathcal{L}_1$ FCS design that improves the prototype with respect to an extended set of criteria.

Table 2. Criteria constraints.

$P2 \leqslant 0.2$	Min	$P9 \leqslant 15$	Pseudo
$P3 \leqslant 0.2$	Min	$P10 \leqslant 300$	Pseudo
$P4 \leqslant 1.02$	Min	$P11 \leqslant 0.25$	Pseudo
$P5 \leqslant 1$	Min	$P12 \leqslant 0.01$	Pseudo
$P6 \leqslant 0.3$	Min	$P13 \leqslant 0.01$	Pseudo
$P7 \leqslant 0.25$	Pseudo	$FQ1 \leqslant 0.1$	Min
$P8 \leqslant 5$	Pseudo	$FQ2 \leqslant 45$	Min

Table 3. Fragment of criteria table.

Criteria		Prototype	Pareto-optimal solutions						
			#241	#281	#329	#409	#649	#825	#993
P2	Min	1.30E−01	1.04E−01	8.40E−02	9.14E−02	8.97E−02	6.03E−02	7.44E−02	5.39E−02
P3	Min	1.54E−01	1.16E−01	1.03E−01	1.06E−01	1.04E−01	8.72E−02	9.51E−02	8.84E−02
P4	Min	1.0E+00	1.00E+00	1.00E+00	1.00E+00	1.00E+00	1.01E+00	1.00E+00	1.00E+00
P5	Min	3.15E−01	5.37E−01	9.36E−01	9.68E−01	6.29E−01	8.63E−01	8.58E−01	6.89E−01
P6	Min	1.49E−01	1.97E−01	2.21E−01	2.58E−01	2.03E−01	1.74E−01	1.94E−01	1.32E−01
P7	Pseudo	1.51E−01	1.65E−01	1.74E−01	1.84E−01	1.72E−01	1.83E−01	1.78E−01	1.75E−01
P8	Pseudo	3.24E+00	3.3E+00	3.29E+00	3.31E+00	3.30E+00	3.31E+00	3.30E+00	3.31E+00
P9	Pseudo	5.96E+00	1.17E+01	7.55E+00	9.1E+00	1.09E+01	1.11E+01	9.36E+00	1.16E+01
P10	Pseudo	1.07E+02	2.42E+02	1.34E+02	1.72E+02	2.16E+02	2.24E+02	1.76E+02	2.44E+02
P11	Pseudo	7.45E−02	7.79E−02	6.02E−02	6.82E−02	8.10E−02	7.72E−02	7.22E−02	7.77E−02
P12	Pseudo	1.01E−04	1.84E−04	1.87E−04	2.08E−04	2.06E−04	2.29E−04	2.14E−04	2.09E−04
P13	Pseudo	3.16E−05	6.18E−05	6.87E−05	8.01E−05	7.00E−05	8.18E−05	7.58E−05	7.03E−05
FQ1	Min	1.23E−02	6.73E−02	9.29E−02	9.74E−02	6.86E−02	9.05E−02	7.80E−02	8.85E−02
FQ2	Min	5.36E+01	4.42E+01	4.35E+01	4.03E+01	4.22E+01	3.79E+01	4.10E+01	4.00E+01

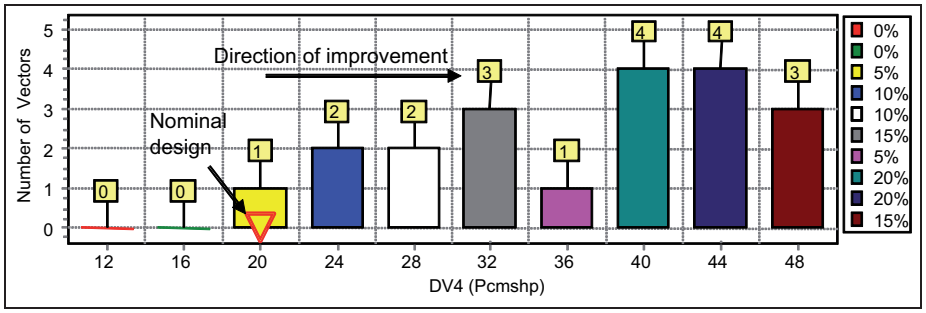

Figure 5. A histogram of *DV4* distribution along with the nominal design (prototype) solution and the direction of improvement (the legend runs left to right and top to bottom, respectively).

Second iteration: design improvement

Based on the analysis of the histograms and criteria table just presented, we adjust the intervals of variation of the DVs as given in Table 4.

The criteria constraints remain unchanged, whereas the design is now to be optimized with respect to the extended set of criteria {*P2, P3, P4, P5, P6, FQ1, FQ2, FQ4, R1*}. All these criteria are to be minimized except for *R1*, which is to be maximized.

Table 4. Refined intervals of design variables.

Design variable	Prototype	Initial intervals of variation of design variables	
		Min	Max
DV1	5.50E+00	5.50E+00	7.00E+00
DV2	8.50E−01	6.50E−01	0.90E+00
DV3	2.00E+01	9.80E+00	4.00E+01
DV4	2.00E+01	1.80E+01	6.50E+01

The results of the second iteration are based on 512 tests, producing 124 feasible solutions. All these solutions are Pareto optimal. The histograms in this second iteration have stronger distributions of the feasible solutions than in the first iteration. Figure 6(a) represents the distribution of 124 solutions for *DV1*.

As a result, analysis of the test table and histograms leads to a stronger set of criteria and pseudocriteria constraints, as presented in Table 5. According to these new constraints, only six solutions are feasible, and all of them are Pareto optimal. The values of the DVs and criteria of the Pareto-optimal solutions are given in Tables 6 and 7, respectively. The new distribution of the feasible solutions for these criteria and pseudocriteria constraints is significantly tighter (Figure 6(b)). The new histograms clearly identify tight intervals for all the DVs in which the optimal solutions lie.

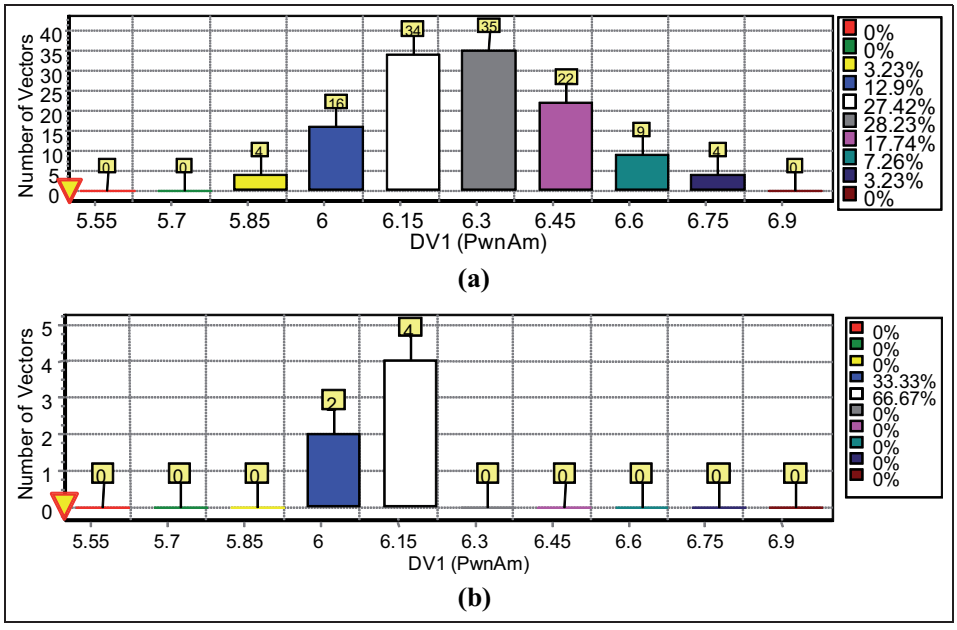

Figure 6. PSI iteration 2. Distribution of feasible solutions of *DV1* with (a) the original criteria constraints and (b) the tightened criteria constraints (the legend runs left to right and top to bottom, respectively).

Further analysis of Table 7 shows that all solutions of this new iteration, as well as design #993 from the first iteration, belong to the very tight intervals of the first and second DVs. The first three parameters (*DV1–DV3*) of #993 and #106 are almost identical. However, one can see that #993, while providing good response of many criteria, does not satisfy the new constraints on criteria *P9* and *P10* (elevator workload). Moreover, design #993 also fails to satisfy the constraint on criterion *FQ3*.

Analysis of the test tables, dependencies of criteria on DVs, and dependencies between criteria allow determining the most preferable solutions. In particular

- Figure 7 shows the influence of the bandwidth of the "matched" low-pass filter (*DV3*) on the (pilot-off-the-loop) trade-off between performance criterion *P2* (*P3* shows the same trend) and robustness *R1* of the augmented aircraft. From this observation, we conclude that criteria *P2* (*P3*) and *R1* are contradictory with respect to the DV *DV3*. This means that improvement of the tracking performance requires an increase in the bandwidth of the low-pass filter, which in turn results in degradation of the time-delay margin of the augmented aircraft. This trade-off is consistent with the predictions of the $\mathcal{L}_1$ adaptive control theory.
- Figure 8 shows the dependencies of the FQ criterion *FQ1* on the DV *DV2*. While the trend seems to indicate that a smaller damping ratio of the state-predictor eigenvalues results in increased (lead) pilot compensation, Figure 8 shows that the new Pareto solutions achieve a 20% reduction in criterion *FQ1* with respect to the prototype design despite having a smaller damping ratio. A similar observation can be made for criterion *FQ2* when analyzed versus DV *DV2*.

The dependency of FQ criteria *FQ1* and *FQ2* obtained in this iteration is also similar to those obtained in the first iteration, thus demonstrating significant improvement of predicted FQ over the prototype design, but now in the extended criteria space.

Table 5. Second iteration, refined criteria constraints.

$P2 \leqslant 0.1$	Min	$P10 \leqslant 200$	Pseudo
$P3 \leqslant 0.15$	Min	$P11 \leqslant 0.1$	Pseudo
$P4 \leqslant 1.02$	Min	$P12 \leqslant 0.01$	Pseudo
$P5 \leqslant 1$	Min	$P13 \leqslant 0.01$	Pseudo
$P6 \leqslant 0.25$	Min	$FQ1 \leqslant 0.1$	Min
$P7 \leqslant 0.2$	Pseudo	$FQ2 \leqslant 45$	Min
$P8 \leqslant 5$	Pseudo	$FQ4 \leqslant 5$	Min
$P9 \leqslant 10$	Pseudo	$R1 \geqslant 80$	Max

Table 6. Second iteration. Table of design variables.

Design variable	Prototype	#993, first iteration	Pareto-optimal solutions					
			#106	#202	#254	#318	#358	#462
DV1	5.50E+00	6.12E+00	6.00E+00	5.99E+00	6.24E+00	6.23E+00	6.10E+00	6.18E+00
DV2	8.50E+00	7.09E−01	7.34E−01	7.49E−01	7.76E−01	7.33E−01	7.81E−01	7.18E−01
DV3	2.0E+01	2.70E+01	2.52E+01	1.67E+01	1.81E+01	2.18E+01	1.69E+01	1.58E+01
DV4	2.0E+01	4.93E+01	3.16E+01	3.20E+01	2.10E+01	2.72E+01	2.57E+01	3.11E+01

Table 7. Second iteration. Table of criteria.

Criteria		Prototype	Pareto-optimal solutions					
			#106	#202	#254	#318	#358	#462
P2	Min	1.30E−001	6.01E−01	8.45E−02	9.17E−02	7.04E−02	9.63E−02	8.28E−02
P3	Min	1.54E−01	9.60E−02	1.13E−01	1.11E−01	9.66E−02	1.18E−01	1.04E−01
P4	Min	1.0E+00	1.00E+00	1.00E+00	1.00E+00	1.00E+00	1.01E+00	1.00E+00
P5	Min	3.15E−01	6.13E−01	6.81E−01	8.85E−01	8.43E−01	7.71E−01	8.63E−01
P6	Min	1.49E−01	1.28E−01	1.67E−01	2.16E−01	1.78E−01	1.94E−01	2.11E−01
P7	Pseudo	1.51E−01	1.68E−01	1.67E−01	1.72E−01	1.76E−01	1.68E−01	1.78E−01
P8	Pseudo	3.24E+00	3.29E+00	3.29E+00	3.29E+00	3.30E+00	3.29E+00	3.31E+00
P9	Pseudo	5.96E+00	9.09E+00	9.1E+00	7.9E+00	9.05E+00	8.43E+00	9.54E+00
P10	Pseudo	1.07E+02	1.77E+02	1.78E+02	1.43E+02	1.72E+02	1.59E+02	1.85E+02
P11	Pseudo	7.45E−02	6.62E−02	6.60E−02	6.09E−02	6.74E−02	6.31E−02	6.95E−02
P12	Pseudo	1.01E−04	1.81E−04	1.70E−04	1.80E−04	2.01E−04	1.69E−04	1.98E−04
P13	Pseudo	3.16E−05	6.02E−05	5.89E−05	6.58E−05	7.13E−05	6.01E−05	7.27E−05
FQ1	Min	1.23E−02	9.93E−02	9.81E−02	9.34E−02	9.26E−02	9.20E−02	9.64E−02
FQ2	Min	5.36E+01	4.33E+01	4.41E+01	4.38E+01	4.14E+01	4.46E+01	4.10E+01
FQ4	Min	4.68E+00	4.08E+00	4.19E+00	3.87E+00	3.88E+00	3.84E+00	3.97E+00
R1	Max	8.50E+01	8.50E+01	1.05E+02	8.00E+01	8.50E+01	9.00E+01	1.00E+02

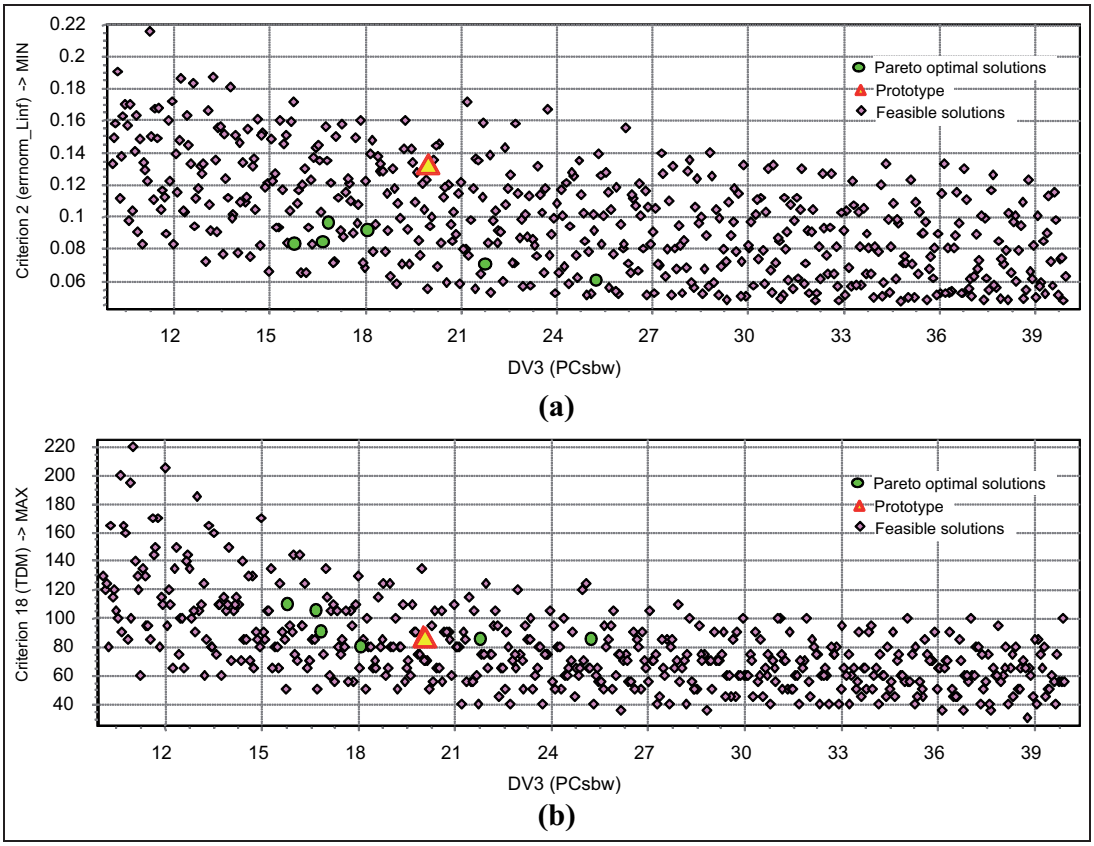

Figure 7. PSI iteration 2. Dependencies of criteria *P2* and *R1* on the design variable *DV3*: (a) criterion *P2* (max AOA deviation) versus design variable *DV3* and (b) criterion *R1* (time-delay margin) versus design variable *DV3*.

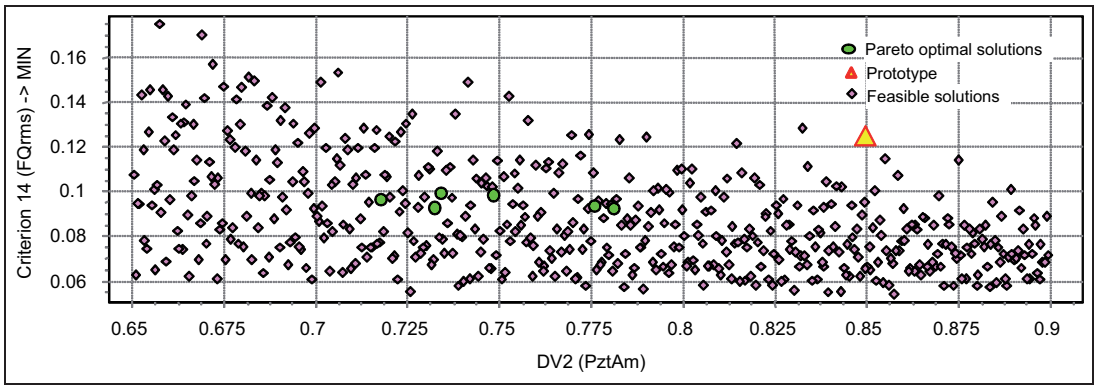

Figure 8. PSI iteration 2. Dependencies of criteria *FQ1* (tracking performance) on the design variable *DV2*.

- Finally, Figure 9 shows the dependency between criteria *P3* and *R1*, which illustrates the fundamental trade-off between performance and robustness of the closed-loop adaptive system with the pilot-off-the-loop. While all the optimal solutions reduce the deviations from the desired response with respect to the prototype design, only three of these solutions exhibit a better time-delay margin than the prototype design (#202, #462) and two exhibit a similar margin (#106, #318).

As a result of iterative two-step correction of initial constraints, six Pareto-optimal solutions have been found. Analysis of these solutions shows that designs #106, #202, #358, and #462 improved the prototype design by six criteria simultaneously. Although all six solutions are practically equivalent, preference is given to the design vector #202, as it overall provides better trade-off between the (predicted) FQ (*FQ1, FQ2*) and the time-delay margin (*R1*), while minimizing the difference with the desired response (Figure 10). We notice that when compared to the time response of the prototype design, the AOA response and the elevator workload of the *optimal* solution #202 provides a faster response (smaller rise time) with a minimal increase in the elevator workload.

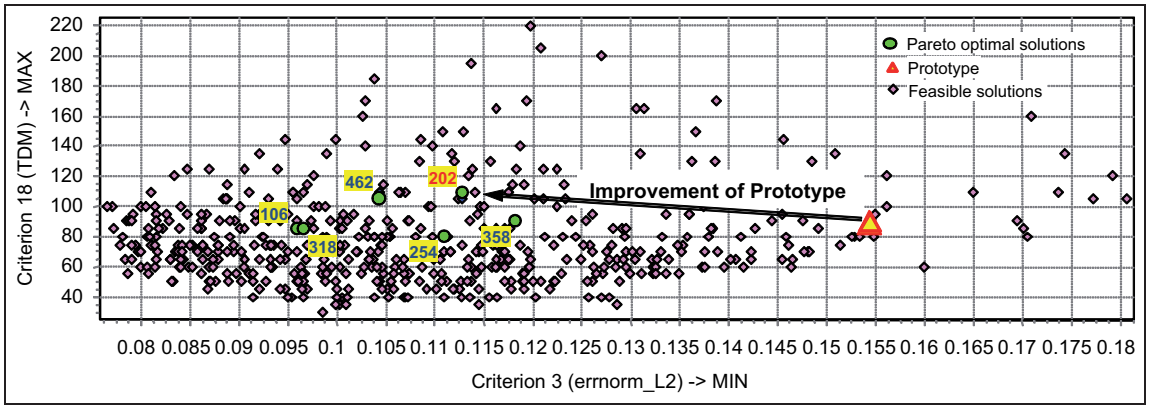

Figure 9. PSI iteration 2. Relation between criteria *R1* (time-delay margin) and *P3* (integral deviation of AOA).

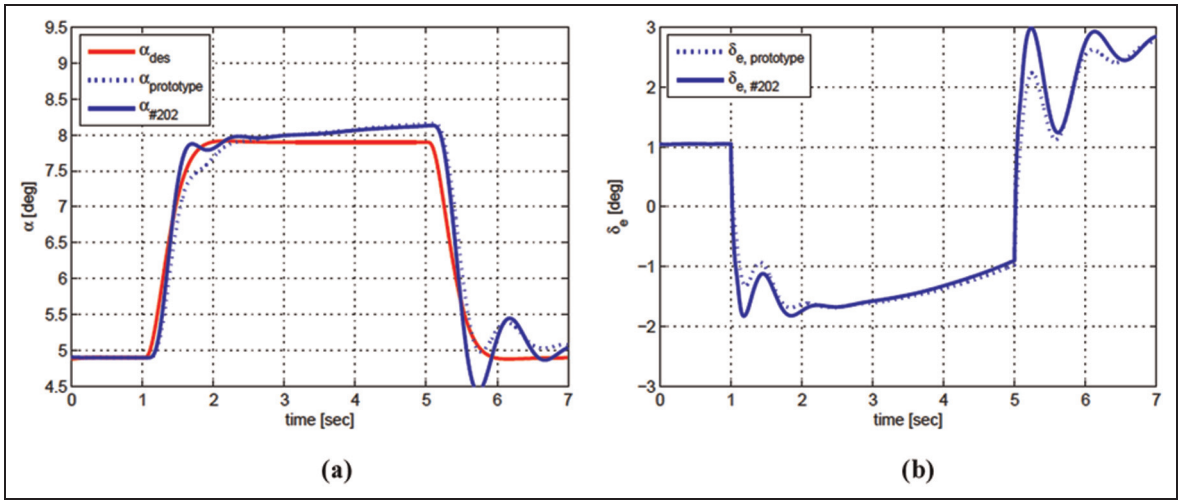

Figure 10. Optimal design #202. 3° AOA step response. (a) Angle of attack, α and (b) elevator deflection, δ_e.

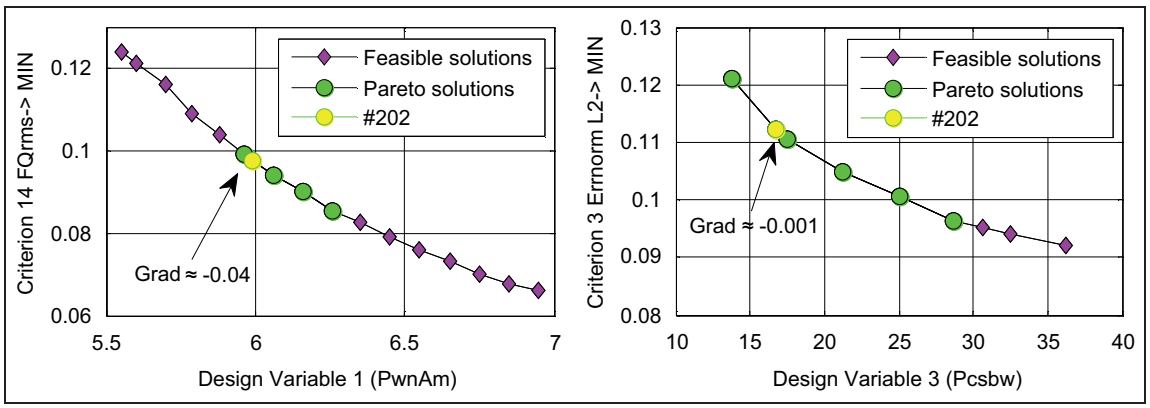

Figure 11. Sensitivity plots.

As the last step, we verify the robustness of design #202 to small variations of the DVs by performing a sensitivity analysis. This analysis calculates a criterion response in the direction defined by a DV in the neighborhood of the optimal solution (in our case, design #202). As an example of this sensitivity analysis, Figure 11 shows the dependency of criterion *FQ1* and desired-model tracking performance *P2* on the DVs *DV1* and *DV3*, respectively; each figure represents the case where only one DV is varied, while the remaining DVs are kept fixed at the optimal value defined by design #202. Compact distribution of the Pareto solutions and smoothness of the criteria confirm the robustness of design #202.

Conclusion

This article presented results of the application of the PSI method and the MOVI software package for the design optimization of the $\mathcal{L}_1$ FCS implemented on the AirSTAR GTM aircraft. In particular, this study has addressed the construction of the feasible solution as well as the improvement of a nominal prototype design. For this purpose, we have formulated and solved an optimization problem with *four DVs*—defining the eigenstructure of the state-predictor state matrix, the bandwidth of the low-pass filter, and the bandwidth of the pilot-command prefilter—and *18 criteria*—characterizing pilot-off-the-loop performance metrics, robustness metrics, as well as FQ and PIO metrics. This study demonstrates that consistent application of the design guidelines of $\mathcal{L}_1$ adaptive control becomes particularly beneficial for the construction of the feasible solution set. Additionally, the results of this study are consistent with the theoretical claims of the theory of $\mathcal{L}_1$ adaptive control in terms of robustness and performance. Moreover, the developed procedure and the obtained results confirm the suitability of the PSI method for the multicriteria optimization of an adaptive flight control law subject to desired control specifications. Finally, we want to emphasize that the insights gained during the optimization process with the MOVI software contributed to the successful flight verification and validation[16] of the designed $\mathcal{L}_1$ adaptive control law at NASA LARC.

Funding

This study was supported by Air Force Office of Scientific Research and NASA.

References

1. Jacklin SA, Lowry MR, Schumann JM, et al. Verification, validation, and certification challenges for adaptive flight-critical control system software. In: *Proceedings of AIAA guidance navigation and control conference and exhibit*, August 2004, AIAA-2004-5258.
2. Wise KA, Lavretsky E and Hovakimyan N. Adaptive control of flight: theory, applications, and open problems. In: *Proceedings of American control conference*, Minneapolis, MN, June 2006, pp.8–10.
3. Jacklin SA. Closing certification gaps in adaptive flight control software. In: *Proceedings of AIAA guidance, navigation and control conference*, Honolulu, HI, August 2008, AIAA-2008-6988.
4. Hovakimyan N and Cao C. *$\mathcal{L}_1$ adaptive control theory*. Philadelphia, PA: Society for Industrial and Applied Mathematics, 2010.
5. Kim KKK and Hovakimyan N. Development of verification and validation approaches for $\mathcal{L}1$ adaptive control: multi-criteria optimization for filter design. In: *Proceedings of AIAA guidance, navigation and control conference*, Toronto, ON, Canada, August 2010.
6. Statnikov RB and Matusov RB. *Multicriteria analysis in engineering*. Dordrecht/Boston/London: Kluwer Academic Publishers, 2002.
7. Sobol IM and Statnikov RB. *Selecting optimal parameters in multicriteria problems*. 2nd ed. Moscow: Drofa, 2006.
8. Statnikov RB and Statnikov AR. *Software package MOVI 1.4 for Windows: user's manual, certificate of registration*.
9. Jordan TL, Langford WM and Hill JS. Airborne subscale transport aircraft research testbed—aircraft model development. In: *Proceedings of AIAA guidance, navigation and control conference*, San Francisco, CA, August 2005, AIAA-2005-6432.
10. Jordan TL, Foster JV, Bailey RM, et al. AirSTAR: a UAV platform for flight dynamics and control system testing. In: *Proceedings of AIAA aerodynamic measurement technology and ground testing conference*, San Francisco, CA, June 2006, AIAA-2006-3307.
11. Foster JV, Cunningham K, Fremaux CM, et al. Dynamics modeling and simulation of large transport airplanes in upset conditions. In: *Proceedings of AIAA guidance, navigation and control conference*, San Francisco, CA, 15–18 August 2005, AIAA-2005-5933.
12. Shah GH. Aerodynamic effects and modeling of damage to transport aircraft. In: *Proceedings of AIAA atmospheric flight mechanics conference*, Honolulu, HI, 18–21 August 2008, AIAA-2008-6203.
13. Stengel R. *Flight dynamics*. Princeton University Press, 2004.
14. MIL Standard:MIL-HDBK-1797. Flying qualities of piloted aircraft. US Department of Defense, 19 December 1997.
15. Xargay E, Hovakimyan N and Cao C. L1 adaptive controller for multi-input multi-output systems in the presence of nonlinear unmatched uncertainties. In: *Proceedings of American control conference, IEEE*, Baltimore, MD, June–July 2010.
16. Xargay E, Hovakimyan N, Dobrokhodov V, et al. L1 adaptive control in flight. In: *Intelligent systems, progress in aeronautics and astronautics series*. American Institute of Aeronautics and Astronautics, 2012.
17. Andersson J. A survey of multi-objective optimization in engineering design. *J Optimiz Theory App* 2000; 36(Issue: LiTH-IKP-R-1097): 1–34.
18. Marler RT and Arora JS. Survey of multi-objective optimization methods for engineering. *Struct Multidiscip O* 2004; 26(6): 369–395.
19. MathWorks. MathWorks—MATLAB and Simulink for technical computing, http://www.mathworks.com/ (2011).
20. Stepanyan V, Krishnakumar K, Nguyen N, et al. Stability and performance metrics for adaptive flight control. In: *Proceedings of AIAA guidance, navigation and control conference*, Chicago, IL, August 2009, AIAA-2009-5965.
21. Bailey RE and Bidlack TJ. *Unified pilot-induced oscillation theory. Volume IV: time-domain Neal-Smith criterion*. Technical report WL-TR-96–3031, December 1995. Air Force Wright Laboratory.
22. Choe R, Xargay E, Hovakimyan N, et al. L1 adaptive control under anomaly: flying qualities and adverse pilot interactions. In: *Proceedings of AIAA guidance, navigation and control conference*, Toronto, ON, Canada, 2010, AIAA-2010-7775.

Appendix I

Notation

A_z	vertical acceleration
p	roll rate
p_{des}	roll-rate desired response
α	angle of attack
α_{cmd}	angle-of-attack pilot command
α_{des}	angle-of-attack desired response
β	angle of sideslip
β_{des}	sideslip-angle desired response
δ_e	elevator deflection command